EPJ Web of Conferences **181**, 01009 (2018) https://doi.org/10.1051/epjconf/201818101009
*EXA2017*

# On the widths and binding energies of $K^-$ nuclear states and the role of $K^-$ multi-nucleon interactions

*Jaroslava* Hrtánková[1,*] and *Jiří* Mareš[1,**]

[1]Nuclear Physics Institute, 250 68 Řež, Czech Republic

**Abstract.** We report on our recent self-consistent calculations of $K^-$ nuclear quasi-bound states using $K^-$ optical potentials derived from chirally motivated meson-baryon coupled channels models [1, 2]. The $K^-$ single-nucleon potentials were supplemented by a phenomenological $K^-$ multi-nucleon interaction term introduced to achieve good fits to $K^-$ atom data. We demonstrate a substantial impact of the $K^-$ multi-nucleon absorption on the widths of $K^-$ nuclear states. If such states ever exist in nuclear many-body systems, their widths are excessively large to allow observation.

## 1 Introduction

The near-threshold $K^-N$ attraction generated by the $\Lambda(1405)$ resonance seems to be strong enough to allow binding of the $K^-$ meson in nuclei. This fact stimulated numerous theoretical studies of $K^-$ nuclear quasi-bound states as well as experimental searches for $K^-$ nuclear clusters [3–5]. However, the question of their binding energies and widths, and even their very existence is still far from being settled. The $K^-N$ interaction near threshold has been recently described within chirally motivated coupled channels meson-baryon interaction models [6–9], parameters of which have been fitted to low-energy experimental data [10, 11]. $K^-N$ scattering amplitudes which enter the construction of $K^-$ optical potentials are strongly energy dependent near and below threshold, i.e., in the region relevant for calculations of kaonic nuclear states. It is important to treat this energy dependence properly [12, 13]. The above chiral meson-baryon interaction models include only $K^-$ absorption on a single-nucleon, $K^-N \to \pi Y$ ($Y = \Sigma, \Lambda$). However, in the nuclear medium, $K^-$ multi-nucleon interactions take place as well [14–16], and have to be considered in realistic evaluations of $K^-$ widths (and to lesser extent also $K^-$ binding energies) in the nuclear medium. Recently, Friedman and Gal [17] supplemented $K^-$ single-nucleon potentials constructed within several chiral coupled channels meson-baryon models by a phenomenological term representing the $K^-$ multi-nucleon interactions. They fitted parameters of this phenomenological term to kaonic data for each meson-baryon interaction model separately. Only the P [7] and KM [6] models were able to reproduce both kaonic data and experimental fractions of $K^-$ absorption at rest [18–20]. In this contribution we apply these two models to calculations of $K^-$ nuclear quasi-bound states in selected nuclei.

In Section 2, we briefly introduce kaon self-energy operator including in-medium modifications of the underlying $K^-N$ scattering amplitudes. We discuss how to incorporate strong

*e-mail: hrtankova@ujf.cas.cz
**e-mail: mares@ujf.cas.cz

energy dependence of the in-medium amplitudes in self-consistent calculations of kaonic nuclear quasi-bound states. In Section 3, we present selected results of our calculations aiming at demonstrating the crucial role played by $K^-$ multi-nucleon interactions in the nuclear medium. A brief summary in Section 4 concludes this contribution.

## 2 Methodology

The interaction of the $K^-$ meson with a nucleus is described by the Klein-Gordon equation

$$\left[\vec{\nabla}^2 + \tilde{\omega}^2_{K^-} - m^2_{K^-} - \Pi_{K^-}(\omega_{K^-}, \rho)\right]\phi_{K^-} = 0 \,, \tag{1}$$

where, $\tilde{\omega}_{K^-} = m_{K^-} - B_{K^-} - \mathrm{i}\Gamma_{K^-}/2 - V_C = \omega_{K^-} - V_C$ with $B_{K^-}$ ($\Gamma_{K^-}$) being the $K^-$ binding energy (width), $m_{K^-}$ denotes the $K^-$ mass, $V_C$ is the Coulomb potential, and $\rho$ is the nuclear density distribution. The kaon self-energy $\Pi_{K^-}$ is constructed from in-medium isospin 0 and 1 $s$-wave amplitudes $F_0$ and $F_1$ in a $t\rho$ form as follows:

$$\Pi_{K^-} = 2\mathrm{Re}(\omega_{K^-})V^{(1)}_{K^-} = -4\pi\frac{\sqrt{s}}{m_N}\left(F_0\frac{1}{2}\rho_p + F_1\left(\frac{1}{2}\rho_p + \rho_n\right)\right) \,, \tag{2}$$

where $V^{(1)}_{K^-}$ is the $K^-$-nucleus optical potential, $m_N$ is the nucleon mass, and the kinematical factor $\sqrt{s}/m_N$ transforms the scattering amplitudes from the two-body frame to the $K^-$-nucleus frame. The proton and neutron density distributions, $\rho_p$ and $\rho_n$, are evaluated within the relativistic mean-field model NL-SH [21].

The in-medium scattering amplitudes were obtained from the free-space amplitudes $f_{K^-p}$ and $f_{K^-n}$, derived within chiral coupled channels meson-baryon interaction models P and KM, using the multiple scattering approach (WRW) [22] in order to account for Pauli correlations. They are of the following form:

$$F_1 = \frac{f_{K^-n}(\sqrt{s})}{1 + \frac{1}{4}\xi_k\frac{\sqrt{s}}{m_N}f_{K^-n}(\sqrt{s})\rho} \,, \quad F_0 = \frac{[2f_{K^-p}(\sqrt{s}) - f_{K^-n}(\sqrt{s})]}{1 + \frac{1}{4}\xi_k\frac{\sqrt{s}}{m_N}[2f_{K^-p}(\sqrt{s}) - f_{K^-n}(\sqrt{s})]\rho} \,, \tag{3}$$

where $\xi_k$ is adopted from Ref. [17].

In Fig. 1, we present the $K^-p$ (top) and $K^-n$ (bottom) amplitudes in the P and KM models, modified by the WRW procedure at saturation density $\rho_0 = 0.17$ fm$^{-3}$, plotted as a function of energy. The corresponding free scattering amplitudes (dotted lines) are presented for comparison. The $K^-p$ in-medium amplitudes are affected significantly by Pauli correlations: the real parts of the amplitudes become attractive in the entire energy region below threshold, and the imaginary parts are considerably lowered. On the other hand, the $K^-n$ amplitudes are modified by Pauli correlations only moderately.

In previous calculations [12, 16], the in-medium $K^-N$ amplitudes in the P model [7] were constructed in a different way. The integration over the intermediate meson-baryon momenta in the underlying Green's function was restricted to a region ensuring the nucleon intermediate energy to be above the Fermi level (denoted further 'Pauli'). In Fig. 2, we compare the Pauli correlated amplitudes with the WRW modified amplitudes in the P model. It is rewarding that both approaches, WRW and Pauli, yield similar $K^-N$ in-medium reduced amplitudes[1] $f^{\mathrm{r}}_{K^-N} = \frac{1}{2}(f^{\mathrm{r}}_{K^-p} + f^{\mathrm{r}}_{K^-n})$ in the subthreshold energy region which is relevant to our calculations of $K^-$ nuclear states. Above threshold, the behavior of Pauli and WRW modified amplitudes is different.

[1] $f^{\mathrm{r}}_{K^-N} = g(p)f_{K^-N}g(p')$, where $g(p)$ is a momentum-space form factor (see Ref. [12])

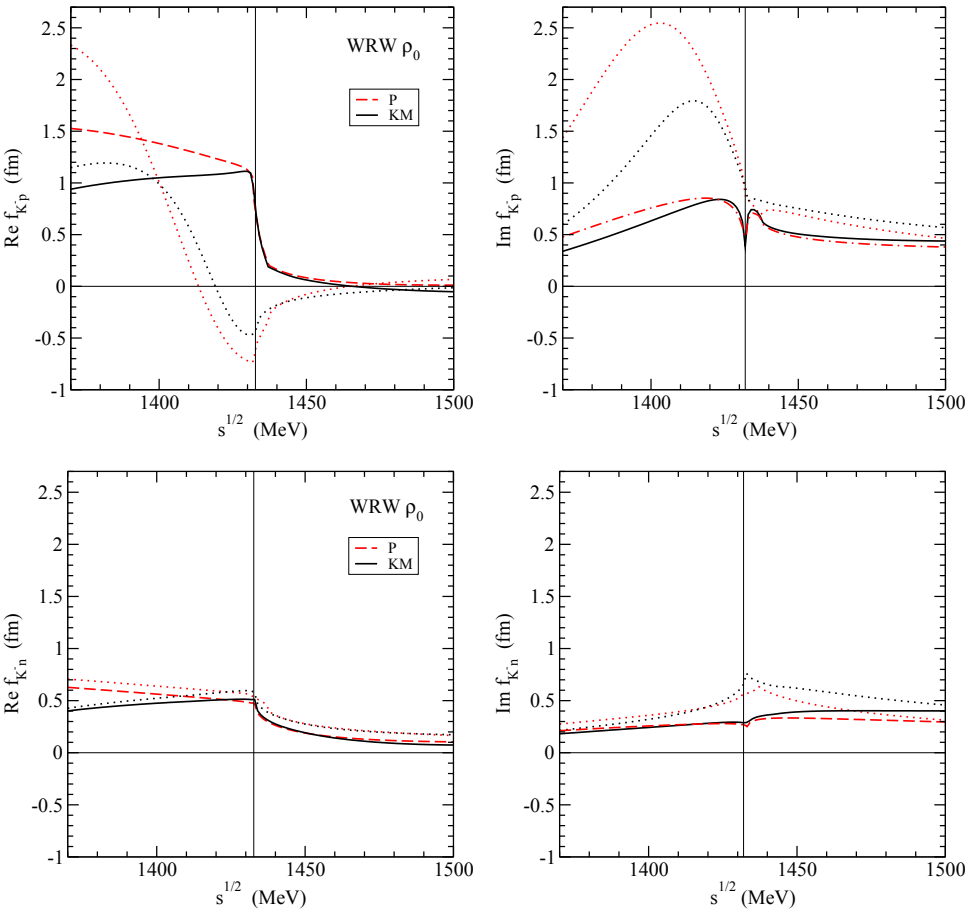


**Figure 1.** Energy dependence of real (left) and imaginary (right) parts of WRW modified $K^-p$ (top) and $K^-n$ (bottom) amplitudes at $\rho_0 = 0.17$ fm$^{-3}$ in the P and KM models. Corresponding free-space amplitudes are shown for comparison (dotted lines).

Important feature of the $K^-p$ scattering amplitudes shown in Figs. 1 and 2 is their strong energy dependence near threshold caused by the presence of the $\Lambda(1405)$ resonance, dynamically generated in chirally motivated coupled channels models. This feature calls for a proper self-consistent treatment during the evaluation of the $K^-$ optical potential. The amplitudes are a function of energy defined by the Mandelstam variable

$$s = (E_N + E_{K^-})^2 - (\vec{p}_N + \vec{p}_{K^-})^2 \,, \tag{4}$$

where $E_N = m_N - B_N$, $E_{K^-} = m_{K^-} - B_{K^-}$ and $\vec{p}_{N(K^-)}$ is the nucleon (kaon) momentum. In the $K^-$-nucleus frame the momentum dependent term is no longer zero and provides additional downward energy shift. The energy shift $\delta\sqrt{s} = \sqrt{s} - E_{th} = \sqrt{s} - (m_N + m_K)$ was expanded in terms of binding and kinetic energies as follows [1, 2]:

$$\delta\sqrt{s} = -B_N\frac{\rho}{\rho} - \beta_N\left[B_{K^-}\frac{\rho}{\rho_{\rm max}} + T_N\left(\frac{\rho}{\rho}\right)^{2/3} + V_C\left(\frac{\rho}{\rho_{\rm max}}\right)^{1/3}\right] + \beta_{K^-}{\rm Re}V_{K^-}(r)\,, \tag{5}$$

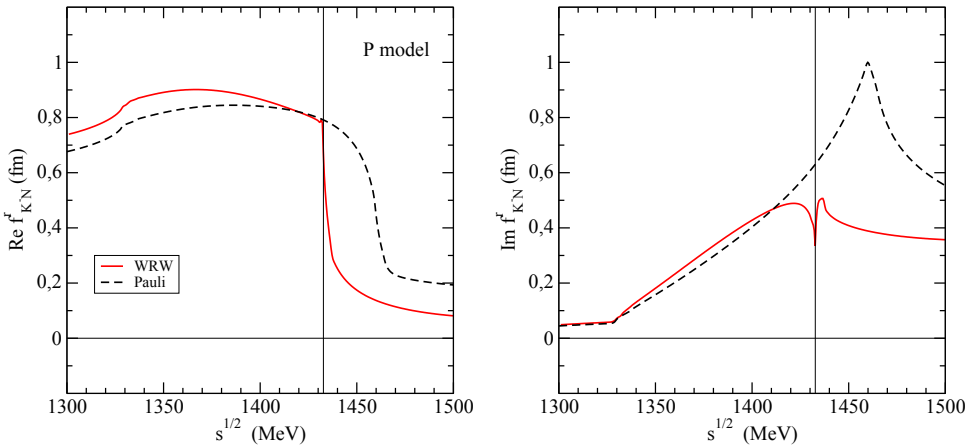


**Figure 2.** Comparison of real (left) and imaginary (right) parts of WRW (full line) and Pauli (dashed line) modified reduced amplitudes $f^{\rm r}_{K^-N} = \frac{1}{2}(f^{\rm r}_{K^-p} + f^{\rm r}_{K^-n})$ plotted as function of energy $\sqrt{s}$ for $\rho_0 = 0.17$ fm$^{-3}$ in the P model (see text for details).

where $B_N = 8.5$ MeV is the average binding energy per nucleon, $\bar{\rho}$ is the average nuclear density, $\rho_{\rm max}$ is the maximal value of the nuclear density, $\beta_{N(K^-)} = m_{N(K^-)}/(m_N + m_{K^-})$ and $T_N = 23$ MeV is the average nucleon kinetic energy in the Fermi Gas Model. The energy shift respects the low-density limit, i. e. $\delta\sqrt{s} \to 0$ as $\rho \to 0$.

The above P and KM models describe only the $K^-$ interactions with a single nucleon. However, $K^-$ interactions with two and more nucleons take place in the medium as well [14, 17]. Therefore, we supplemented the $K^-$ single-nucleon potential $V^{(1)}_{K^-}$ from Eq. (2) with a phenomenological optical potential $V^{(2)}_{K^-}$ describing the $K^-$ multi-nucleon interactions:

$$2{\rm Re}(\omega_{K^-})V^{(2)}_{K^-} = -4\pi B(\frac{\rho}{\rho_0})^\alpha\rho\,. \tag{6}$$

The parameters of the phenomenological potential, complex amplitude $B$ and positive exponent $\alpha$ listed in Table 1, were recently fitted by Friedman and Gal [17] to kaonic atom data for each $K^-N$ interaction model separately. Moreover, the total $K^-$ optical potential, $V_{K^-} = V^{(1)}_{K^-} + V^{(2)}_{K^-}$, was confronted with branching ratios of $K^-$ absorption at rest from bubble chamber experiments [18–20] and the P and KM models discussed in this contribution were found to be the only two interaction models capable of reproducing both experimental constraints simultaneously.

The kaonic atom data probe the $K^-$ optical potential up to at most $\sim 50\%$ of the nuclear density [17]. Further inside the nucleus, the shape of the potential is just a matter of ex-

**Table 1.** Values of the complex amplitude $B$ and exponent $\alpha$ used to evaluate $V^{(2)}_{K^-}$ for chiral meson-baryon interaction models considered in this work.

| | P1 | KM1 | P2 | KM2 |
|---|---|---|---|---|
| $\alpha$ | 1 | 1 | 2 | 2 |
| Re$B$ (fm) | $-1.3 \pm 0.2$ | $-0.9 \pm 0.2$ | $-0.5 \pm 0.6$ | $0.3 \pm 0.7$ |
| Im$B$ (fm) | $1.5 \pm 0.2$ | $1.4 \pm 0.2$ | $4.6 \pm 0.7$ | $3.8 \pm 0.7$ |

trapolation to higher densities. Therefore, we considered two options in our calculations: a) we applied the formula (6) in the entire nucleus (full density option - FD) b) we fixed the potential $V^{(2)}_{K^-}$ at constant value $V^{(2)}_{K^-}(0.5\rho_0)$ for $\rho(r) \geq 0.5\rho_0$ (half density limit - HD).

## 3 Results

The formalism outlined in the previous section was adopted to self-consistent calculations of $K^-$ nuclear quasi-bound states in various nuclei across the periodic table. Here we present only few selected results, for more details see Refs. [1, 2]).

The self-consistently evaluated energy shift $\delta\sqrt{s}$ from Eq (5) is strongly density dependent which plays important role in calculations of kaonic nuclear, as well as atomic states. Figure 3 illustrates the strong density dependence of $\delta\sqrt{s}$ in $^{208}$Pb, calculated self-consistently within the P and KM models augmented by the FD variant of $V^{(2)}_{K^-}$ with $\alpha = 1$ (P1, KM1) and $\alpha = 2$ (P2, KM2). The P1 and KM1 models yield smaller energy shift with respect to the $K^-N$ threshold than the original single-nucleon potentials $V^{(1)}_{K^-}$ (P and KM). The P2 and KM2 models yield energy shifts closer to the single-nucleon potentials. The energy shift for the FD option is in any case shallower than for the original $K^-$ single-nucleon potential owing to very strong absorption. It is to be noted that the P and KM models supplemented with various versions of the multi-nucleon interaction term could be regarded as equivalent since they all lie in corresponding uncertainty bands and describe kaonic atom data equally well.

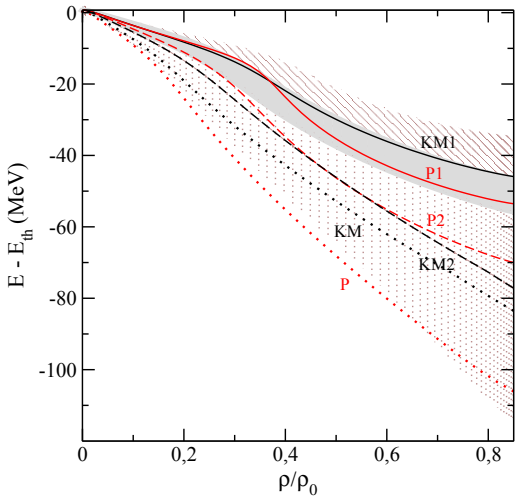


**Figure 3.** Subthreshold energies probed in the $^{208}$Pb+$K^-$ nucleus as a function of relative density $\rho/\rho_0$, calculated self-consistently in the single-nucleon $K^-N$ amplitude models P and KM (dotted lines), supplemented by the FD variant of $V^{(2)}_{K^-}$ with $\alpha = 1$ (full lines) and $\alpha = 2$ (dashed lines). The shaded areas stand for uncertainties.

In Fig. 4, we present real (left) and imaginary (right) parts of the total $K^-$ potential in $^{208}$Pb, calculated self-consistently in the KM1 and KM2 models for the HD and FD options of the multi-nucleon potential $V^{(2)}_{K^-}$. The gray shaded areas stand for uncertainties in $V^{(2)}_{K^-}$ due to the complex parameter $B$ (see Table 1). The underlying chirally-inspired $K^-$ single-nucleon potential (denoted by 'KN') are shown for comparison. The real parts of the $K^-$ optical potential are affected by multi-nucleon interactions markedly less than its imaginary

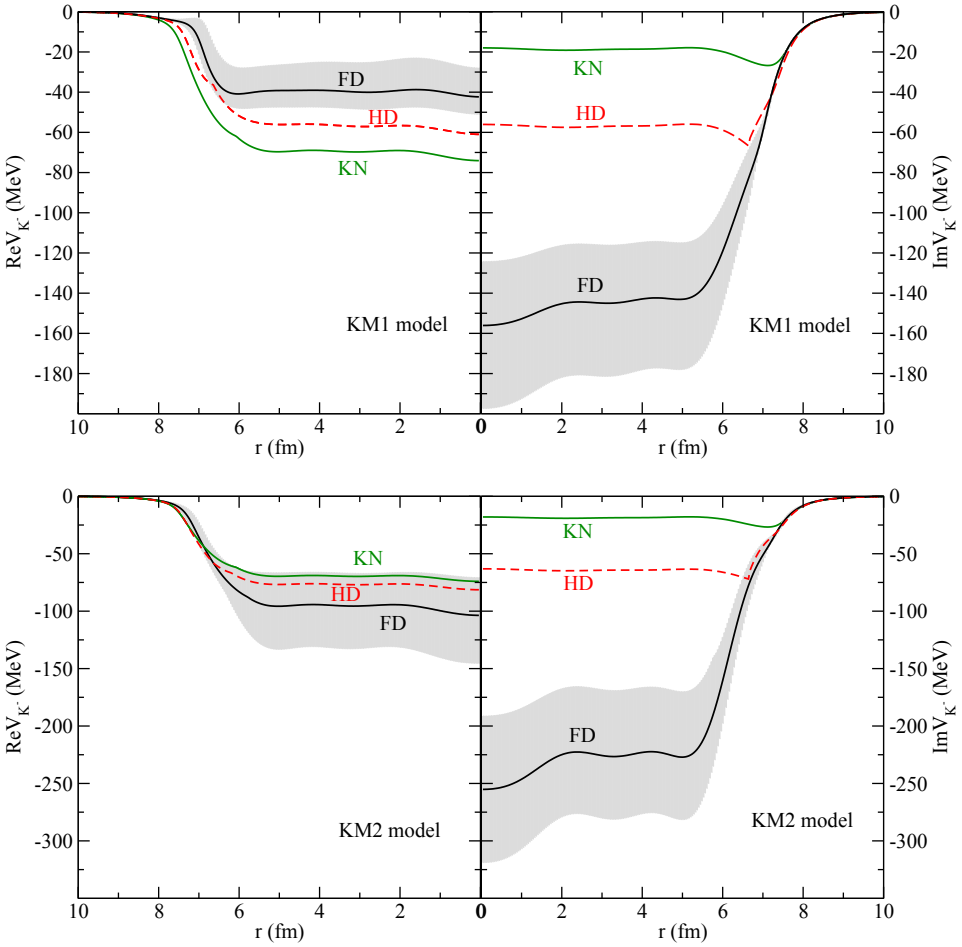


**Figure 4.** The real (left) and imaginary (right) part of the $K^-$ optical potential in $^{208}$Pb, calculated self-consistently in the KM1 (top) and KM2 (bottom) model, for the HD and FD versions of the $K^-$ multi-nucleon potential (see text for details). The shaded areas stand for uncertainties. The single-nucleon $K^-$ potential (KN, green solid lines) calculated in the KM model is shown for comparison.

parts in all considered models. In the KM1 model, the FD and HD options yield Re$V_{K^-}$ shallower than the original single-nucleon $V^{(1)}_{K^-}$ potential. The same holds for the P1 and P2 models (not shown in the figure). In the KM2 model, the overall $K^-$ real potential is deeper than the underlying $K^-$ single-nucleon potential due to the positive sign of Re$B$. The Re$V_{K^-}$ potentials for HD and FD options differ between each other up to $\approx$ 20 MeV in each interaction model. On the other hand, the imaginary parts of $V_{K^-}$ exhibit much larger dispersion for different versions of $V^{(2)}_{K^-}$, as illustrated in Fig. 4, right panels. The $K^-$ multi-nucleon absorption significantly deepens the imaginary part of the $K^-$ optical potential. For the FD option of $V^{(2)}_{K^-}$, the KM model yields $|\mathrm{Im}V_{K^-}| \gg |\mathrm{Re}V_{K^-}|$ inside the nucleus for both values of $\alpha$, even when the uncertainties of the $K^-$ multi-nucleon potential are taken into account. The same holds for the P model (not shown in the figure).

The particular role of $K^-$ single- and multi-nucleon absorptions with respect to the nuclear density is illustrated in Fig. 5. Here we compare individual contributions of $K^-$ single

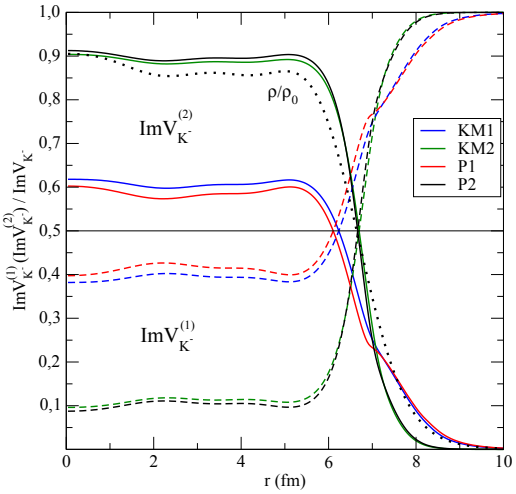


**Figure 5.** The ratio of $\mathrm{Im}V^{(1)}_{K^-}$ (dashed line) and $\mathrm{Im}V^{(2)}_{K^-}$ (solid line) potentials to the total $K^-$ imaginary potential $\mathrm{Im}V_{K^-}$ as a function of radius, calculated self-consistently for $^{208}$Pb+$K^-$ system within different $K^-N$ interaction models and FD option for the $K^-$ multi-nucleon potential. The relative nuclear density $\rho/\rho_0$ (dotted line) is shown for comparison.

nucleon and multi-nucleon absorptions to the total $K^-$ absorption, expressed as a fraction of $\mathrm{Im}V^{(1)}_{K^-}$ and $\mathrm{Im}V^{(2)}_{K^-}$ with respect to the total imaginary $K^-$ potential $\mathrm{Im}V_{K^-}$ in $^{208}$Pb, calculated self-consistently within the P and KM models for the FD option of $V^{(2)}_{K^-}$. The density $\rho/\rho_0$ (thin dotted line) is shown for comparison. Since the range of the corresponding potentials is different, the relative contributions of $\mathrm{Im}V^{(1)}_{K^-}$ and $\mathrm{Im}V^{(2)}_{K^-}$ to the $K^-$ absorption are changing with radius (density). At the nuclear surface, the $K^-$ absorption on a single nucleon dominates, while it is reduced in the nuclear interior due to vicinity of $\pi\Sigma$ threshold and the multi-nucleon absorption prevails. The models with $\alpha = 2$ yield lower relative fraction of the single-nucleon $K^-N$ absorption in the nuclear medium than the models with $\alpha = 1$. It is due to the self-consistent value of $\sqrt{s}$ at $\rho_0$ which is closer to the $K^-N \to \pi\Sigma$ threshold in the case with $\alpha = 2$ (see Fig. 3). It is to be noted that both options for multi-nucleon potential, HD and FD, yield similar fraction of the $K^-$ single-nucleon and multi-nucleon absorption inside the nucleus.

Finally, in Table 2 we present $1s$ $K^-$ binding energies $B_{K^-}$ and widths $\Gamma_{K^-}$, calculated within the P and KM models. For comparison, we show also $K^-$ binding energies and widths calculated only with the chirally-inspired $K^-$ single-nucleon potentials. The $K^-$ multi-nucleon interactions cause radical increase of $K^-$ widths, while $K^-$ binding energies change much less. The HD option of the $V^{(2)}_{K^-}$ potential yields $K^-$ widths of order $\sim$ 100 MeV and the binding energies much smaller than the corresponding widths in most nuclei. The FD multi-nucleon potential $V^{(2)}_{K^-}$ even does not predict any antikaon bound state in the majority of nuclei. We found $1s$ $K^-$ quasi-bound states in $^{90}$Zr and $^{208}$Pb but the corresponding $K^-$ binding energies are small and the widths are one order of magnitude larger than the binding energies [2].

[2]For the FD variant of the P2 model, we had to scale huge imaginary part $\mathrm{Im}V_{K^-}$ by factor 0.8 in order to get fully converged self-consistent solution of Eq. 1.

**Table 2.** 1s $K^-$ binding energies and widths (in MeV) in selected nuclei calculated using the single-nucleon $K^-N$ KM amplitudes (denoted KN); plus a phenomenological amplitude $B(\rho/\rho_0)^\alpha$, where $\alpha = 1$ and 2, for half-density limit (HD) and full density option (FD) (see text for details).

| KM model | | | $\alpha = 1$ | | $\alpha = 2$ | |
|---|---|---|---|---|---|---|
| | | KN | HD | FD | HD | FD |
| $^{12}$C | $B_{K^-}$ | 45 | 34 | not | 48 | not |
| | $\Gamma_{K^-}$ | 44 | 114 | bound | 125 | bound |
| $^{16}$O | $B_{K^-}$ | 45 | 34 | not | 48 | not |
| | $\Gamma_{K^-}$ | 40 | 109 | bound | 121 | bound |
| $^{40}$Ca | $B_{K^-}$ | 59 | 50 | not | 64 | not |
| | $\Gamma_{K^-}$ | 37 | 113 | bound | 126 | bound |
| $^{90}$Zr | $B_{K^-}$ | 69 | 56 | 17 | 72 | 30 |
| | $\Gamma_{K^-}$ | 36 | 107 | 312 | 120 | 499 |
| $^{208}$Pb | $B_{K^-}$ | 78 | 64 | 33 | 80 | 53 |
| | $\Gamma_{K^-}$ | 38 | 108 | 273 | 122 | 429 |

| P model | | | $\alpha = 1$ | | $\alpha = 2$ | |
|---|---|---|---|---|---|---|
| | | KN | HD | FD | HD | FD |
| $^{12}$C | $B_{K^-}$ | 64 | 50 | not | 64 | not |
| | $\Gamma_{K^-}$ | 28 | 96 | bound | 122 | bound |
| $^{16}$O | $B_{K^-}$ | 64 | 50 | not | 63 | not |
| | $\Gamma_{K^-}$ | 25 | 94 | bound | 117 | bound |
| $^{40}$Ca | $B_{K^-}$ | 81 | 67 | not | 82 | not |
| | $\Gamma_{K^-}$ | 14 | 95 | bound | 120 | bound |
| $^{90}$Zr | $B_{K^-}$ | 90 | 74 | 19 | 87 | not |
| | $\Gamma_{K^-}$ | 12 | 88 | 340 | 114 | bound |
| $^{208}$Pb | $B_{K^-}$ | 99 | 82 | 37 | 96 | 47* |
| | $\Gamma_{K^-}$ | 14 | 92 | 302 | 117 | 412* |

* the solution of Eq. 1 for $\mathrm{Im}V_{K^-}$ scaled by factor 0.8

## 4 Summary

In this contribution, we reported on our most recent self-consistent calculations of $K^-$ nuclear quasi-bound states performed using a $K^-$ single-nucleon potential derived within two chirally motivated coupled channels meson-baryon interaction models P and KM, supplemented by a phenomenological potential representing $K^-$ multi-nucleon interactions. The applied models were recently fitted to kaonic atom data and confronted with the branching ratios of $K^-$ single-nucleon absorption at rest [17]. We demonstrated that the $K^-$ multi-nucleon absorption gives rise to substantial increase of $K^-$ absorption widths. In vast majority of nuclei the widths of $K^-$ nuclear quasi-bound states exceed considerably corresponding $K^-$ binding energies. Identification of such states in experiment seems thus highly unlikely.

## Acknowledgements

We thank E. Friedman and A. Gal for valuable discussions. This work was supported by the GACR Grant No. P203/15/04301S.

## References

[1] J. Hrtánková, J. Mareš, Phys. Lett. **B 770**, 342 (2017).
[2] J. Hrtánková, J. Mareš, Phys. Rev. **C 96**, 015205 (2017).
[3] W. Weise, Nucl. Phys. **A 835** (2010) 51, and references therein.
[4] A. Gal, E. V. Hungerford, D. J. Millener, Rev. Mod. Phys. **88**, 035004 (2016), and references therein.
[5] N. V. Shevchenko, Few-Body Syst. **58**, 6 (2017), and references therein.
[6] Y. Ikeda, T. Hyodo and W. Weise, Nucl. Phys. **A 881**, 98 (2012).
[7] A. Cieplý, J. Smejkal, Nucl. Phys. **A 881**, 115 (2012).
[8] Z. H. Guo, J. A. Oller, Phys. Rev. **C 87**, 035202 (2013).
[9] M. Mai and U.-G. Meißner, Nucl. Phys. **A 900**, 51 (2013).
[10] A. D. Martin, Nucl. Phys. **B 179**, 33 (1981), and references therein.
[11] M. Bazzi et al (SIDDHARTA Collaboration), Phys. Lett. **B 704**, 113 (2011).
[12] A. Cieplý, E. Friedman, A. Gal, D. Gazda and J. Mareš, Phys. Lett. **B 702**, 402 (2011).
[13] A. Cieplý, E. Friedman, A. Gal, D. Gazda and J. Mareš, Phys. Rev. **C 84**, 045206 (2011).
[14] J. Mareš, E. Friedman, A. Gal, Phys. Lett. **B 606**, 295 (2005).
[15] J. Mareš, E. Friedman, A. Gal, Nucl. Phys. **A 770**, 84 (2006).
[16] D. Gazda, J. Mareš, Nucl. Phys. **A 881**, 159 (2012).
[17] E. Friedman, A. Gal, Nucl. Phys. **A 959**, 66 (2017).
[18] H. Davis, F. Oppenheimer, W. L. Knight, F. R. Stannard, O. Treutler, Nuovo Cimento **53 A**, 313 (1968).
[19] J. W. Moulder, N. E. Garret, L. M. Tucker, W. M. Bugg, G. T. Condo, H. O. Cohn, R. D. McCulloch, Nucl. Phys. **B 35**, 332 (1971).
[20] C. Vander Velde-Wilquet, J. Sacton, J. H. Wickens, D. N. Tovee, D. H. Davis, Nuovo Cimento **39 A**, 539 (1977).
[21] M. M. Sharma, M. A. Nagarajan, and P. Ring, Phys. Lett. **B 312**, 377 (1993).
[22] T. Wass, M. Rho and W. Weise, Nucl. Phys. **A 617**, 449 (1997).